IEEE Access
Multidisciplinary | Rapid Review | Open Access Journal

Received August 16, 2019, accepted September 9, 2019, date of publication September 27, 2019, date of current version October 10, 2019.

Digital Object Identifier 10.1109/ACCESS.2019.2944137

Non-Pilot Protection of the Inverter-Dominated Microgrid

HOUMAN LAHIJI[1], (Member, IEEE), FIROUZ BADRKHANI AJAEI[1], (Member, IEEE), AND RYAN E. BOUDREAU[2]

[1]Electrical and Computer Engineering Department, Western University, London, ON N6A 5B9, Canada
[2]Protection and Automation Department, Hydro One Networks Inc., Toronto, ON M5G 1P5, Canada

Corresponding author: Firouz Badrkhani Ajaei (fajaei@uwo.ca)

This work was supported by the Hydro One Networks Inc.

ABSTRACT Without utilizing costly communication systems, the existing protection strategies fail to reliably detect the occurrence and direction of faults in the inverter-dominated microgrid. To address this issue, this paper introduces a selective and reliable non-pilot protection strategy for the inverter-dominated microgrid. The proposed protection strategy (i) does not require communication signals, (ii) incorporates phase- and sequence-domain protective elements for reliable detection of symmetrical and asymmetrical faults, (iii) improves the existing sequence-domain directional elements and effectively utilizes them for accurate determination of the fault direction in the presence of inverter-interfaced distributed energy resources, (iv) selectively protects the inverter-dominated microgrid against internal and external faults, (v) is robust against the grid-connection mode of the microgrid, and (vi) enables fuse protection of laterals and non-critical circuits. The acceptable performance of the proposed protection strategy is verified through comprehensive fault studies conducted on a realistic study system simulated in the PSCAD/EMTDC software environment. This paper also demonstrates that the proposed protection strategy can be implemented using an off-the-shelf digital relay.

INDEX TERMS Inverter-dominated microgrid, protection, relay, fault detection, negative-sequence directional element.

I. INTRODUCTION

The proliferation of the alternating current (AC) microgrid has been constrained by the lack of a cost-effective, selective, and reliable strategy for its protection against faults [1]–[4]. The protection strategies used in traditional distribution networks are not generally applicable to microgrids [4], [5]. The protection challenges are further complicated in the inverter-dominated microgrid to which the majority, if not all, of the distributed energy resources (DERs) are interfaced through inverters [2], [6], [7]. The issue is threefold. First, the conventional over-current (OC) relays may fail to detect the limited fault currents contributed by the inverter-interfaced DERs (IIDERs) [2]–[4], [7], [8]. Second, coordinating the OC relays in the inverter-dominated microgrid is challenging, due to the significantly different fault current levels under the grid-connected and islanded operation modes [2]–[4], [9]. Third, the conventional phase- and sequence-domain directional elements fail to accurately determine the fault direction in the inverter-dominated microgrid, under specific operating conditions, as demonstrated in this paper.

Different microgrid protection strategies have been proposed to address these issues. The differential protection strategy [6], [10] requires current measurement at all boundaries of its protection zone [3], [5], which may be costly and impractical in microgrids with multiple feeder sections and dispersed DERs [3]. The adaptive protection schemes [11]–[14] resolve the fault detection and protection coordination issues but require prior knowledge of all possible configurations, operation modes, and the associated fault current levels [5], [14]. The voltage-based protection strategy of [15] is intrinsically robust against variations in the fault current levels but suffers from lower sensitivity to faults in the grid-connected microgrid [5]. A pilot protection scheme is used in [1] to enable coordination of directional OC relays using dual settings. A common disadvantage of the aforementioned protection strategies is that they all require

The associate editor coordinating the review of this manuscript and approving it for publication was Bin Zhou.

remote communication which can be prohibitively expensive, especially in large-scale microgrids [3], [5]. Relying on communication networks also increases vulnerability to communication failure and cyber-attacks [14].

The cost and reliability issues associated with the communication-assisted protection strategies can be avoided by utilizing non-pilot protection strategies, i.e., relays that do not require communication signals. However, the non-pilot protection strategies that have been introduced for microgrid applications [2], [6], [7], [16]–[18] do not reliably protect inverter-dominated microgrids under all possible operating conditions and fault scenarios. The harmonic measurement method of [2] requires special inverters for fifth harmonic injection and is only applicable to the islanded microgrid. A wavelet transform-based data mining strategy is proposed in [16] for fault detection and classification. This strategy requires building a data mining model based on the knowledge of all possible variations in the microgrid fault behavior, which is usually not practical. The symmetrical component-based protection method of [17] only detects asymmetrical faults [7], [18] and is only applicable to unigrounded microgrids [19].

The non-pilot directional protection strategies introduced in [6], [7], [18] effectively resolve the protection coordination issues by using the definite-time grading technique. However, these protection strategies have not been devised for inverter-dominated microgrids. The study systems of [6], [7], and [18] contain sizable synchronous generators. As a result, the fault detection methods utilized in [7] and [18] suffer from low sensitivity to resistive ground faults in the islanded inverter-dominated microgrid. The protection strategy of [6], which utilizes phase OC and negative-sequence OC elements, reliably detects asymmetrical faults but has low sensitivity to symmetrical faults in the islanded inverter-dominated microgrid. In addition, the protection strategies of [6], [7], and [18] would fail to accurately determine the asymmetrical fault direction under specific operating conditions in the inverter-dominated microgrid, as explained in Section II.

This paper introduces a non-pilot protection strategy that effectively addresses the aforementioned issues related to fault detection, fault direction identification, and protection coordination, in the inverter-dominated microgrid. The proposed protection strategy incorporates (i) phase- and sequence-domain protective elements for reliable detection of symmetrical and asymmetrical faults, (ii) improved positive and negative sequence-domain directional elements for reliable detection of the fault direction, and (iii) a protection coordination strategy inspired by the definite-time grading technique of [6], [7], [18], for selective protection under both grid-connected and islanded operation modes.

Comprehensive fault studies are conducted on a detailed model of a realistic study system, in the PSCAD software environment. The results indicate that the proposed protection strategy operates reliably and selectively in an inverter-dominated microgrid, under both grid-connected and islanded operation modes. The practicality of the proposed protection strategy is also verified by implementing it in an off-the-shelf digital relay and demonstrating its desirable operation using an industrial relay testing platform.

II. DIRECTIONAL PROTECTION ELEMENTS

Directional protection elements have been widely used in traditional power systems, and their capabilities and shortcomings are well known to the research community. However, the consequences of utilizing these protective elements in the inverter-dominated microgrid are yet to be fully understood. This section briefly reviews the operating principles of the existing directional protection elements and highlights a misconception that leads to incorrect detection of the asymmetrical fault direction under specific conditions in the inverter-dominated microgrid. The information provided in this section constitutes the foundation of the microgrid protection strategy proposed in the next section.

The phase directional element discriminates between forward and reverse faults based on the phase-domain voltages and currents. This element may fail to accurately detect the fault direction if the current contains a large zero-sequence component [20], [21]. The shortcomings of the phase directional element have led to the development of sequence directional elements, which usually assess the phase angle differences between the sequence-domain voltages and currents to identify the fault direction. Each of the positive-, negative-, and zero-sequence directional elements detects the directions of specific types of faults more accurately [3], [20].

A. SYMMETRICAL FAULTS

The positive-sequence directional element (PSDE) can be used to determine the symmetrical fault direction [3], [20], [22]. Assume a symmetrical fault happens on a line connecting two areas of a microgrid, Fig. 1, where the per-unit distance to the fault is denoted by $0 \leq m \leq 1$. Each of the areas A and B may contain sources, loads, lines, and the point of common coupling (PCC) with the utility grid. Representing these areas with the associated Thevenin equivalent circuits results in the simplified, yet accurate, circuit diagram of Fig. 2. In Fig. 2, Z_L, Z_A, and Z_B respectively represent the line impedance and the Thevenin equivalent impedances of the areas A and B. Assume the relays at the two ends of the faulted line, i.e., $\mathrm{R_A}$ and $\mathrm{R_B}$, utilize PSDEs with the reference directions shown in Fig. 2. The positive-sequence network corresponding to the symmetrical fault scenario is shown in Fig. 3, where the subscript 1 identifies the positive-sequence quantities and parameters.

The positive-sequence voltage phasors measured by the $\mathrm{R_A}$ and the $\mathrm{R_B}$ are defined by (1) and (2), respectively.

$$V_{R_A} = V_{1A} = m \times Z_{1L} \times I_{1A} + Z_f \times (I_{1A} + I_{1B}) \quad (1)$$

$$V_{R_B} = V_{1B} = (1 - m) \times Z_{1L} \times I_{1B} + Z_f \times (I_{1A} + I_{1B}) \quad (2)$$

Neglecting the fault impedance ($Z_f \approx 0$), the approximate positive-sequence current seen by the $\mathrm{R_A}$ and the $\mathrm{R_B}$ are:

$$I_{R_A} = I_{1A} \approx \frac{V_{1A}}{m \times Z_{1L}} \quad (3)$$

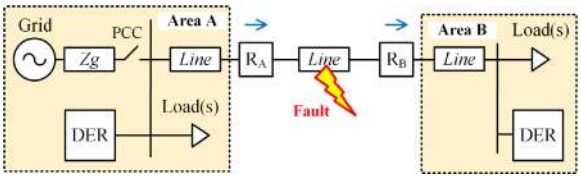

FIGURE 1. Line fault in a typical inverter-dominated microgrid.

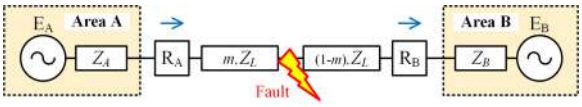

FIGURE 2. Simplified representation of the faulted system of Fig. 1.

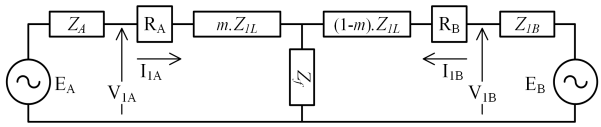

FIGURE 3. Positive-sequence network corresponding to the faulted microgrid of Fig.1, when the fault is symmetrical.

$$I_{R_B} = -I_{1B} \approx -\frac{V_{1B}}{(1-m) \times Z_{1L}} \tag{4}$$

The PSDEs of the R_A and the R_B measure the angles [22]:

$$\angle V_{R_A} - \angle I_{R_A} = \angle (m \times Z_{1L}) = \angle Z_{1L}, \tag{5}$$

$$\angle V_{R_B} - \angle I_{R_B} = \angle (-(1-m) \times Z_{1L}) = \angle -Z_{1L}. \tag{6}$$

As indicated by (5) and (6), there is approximately 180 degrees difference between the angles of the positive-sequence impedances seen by a relay, under forward and reverse symmetrical faults. This large difference is used by the PSDE to reliably determine the fault direction [22]. The fault is assumed to be in the forward direction if the measured positive-sequence impedance angle falls in a half-plane of ± 90 degrees around the element characteristics angle (ECA), which is typically set at $\angle Z_{1L}$ to maximize the security margin [20], [22]. Fig. 4 shows the forward and reverse operating characteristics of the PSDE and the positive-sequence impedances measured by the relays R_A and R_B, when the fault of Fig.1 is symmetrical [22], [23].

It is reported in [3], [21], [22], [24] that setting the ECA at $\angle Z_{1L}$ may cause false determination of the symmetrical fault direction in systems with high penetration of DERs, due to the associated reactive power injection. To prevent such issues, setting the ECA of the PSDE at values smaller than the $\angle Z_{1L}$ is proposed in [22] and [24].

B. ASYMMETRICAL FAULTS

The zero-sequence directional element (ZSDE) and the negative-sequence directional element (NSDE) have been widely used to determine asymmetrical fault direction in traditional power systems [3], [20], [21], [25]. The ZSDE (i) does not identify the directions of phase-to-phase faults, (ii) has different design requirements depending on the system grounding strategy [3], [26], which drastically varies between different microgrids [19], (iii) is prone to failure due to zero-sequence mutual coupling, and (iv) requires substation transformer neutral current measurement or broken-delta-connected voltage transformers [25], [26]. The NSDE has been available in relays since 1990s and widely utilized by utilities, e.g., BC Hydro, [25], and does not suffer from the aforementioned issues [3], [20], [21], [25], [26]. Thus, the rest of this section is focused on the operating principles and application challenges of the NSDE.

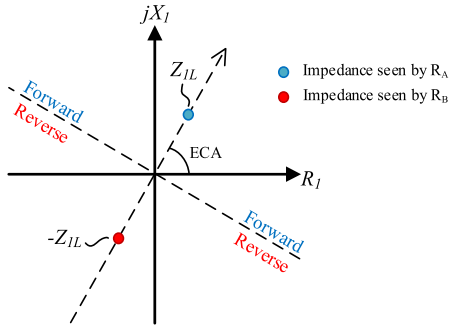

FIGURE 4. Operating characteristics of the PSDE and the positive-sequence impedances seen by R_A and R_B when the fault of Fig. 1 is symmetrical.

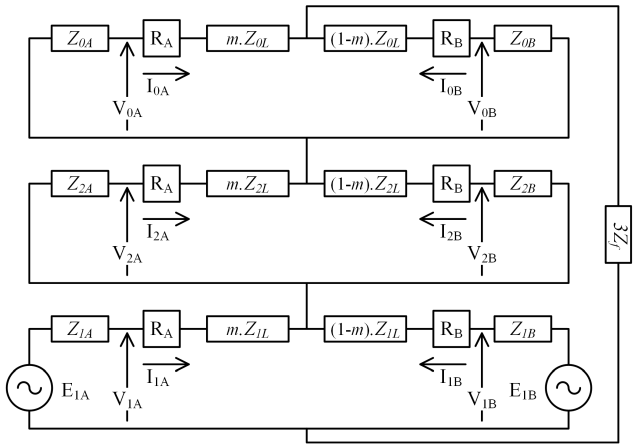

FIGURE 5. Sequence network corresponding to the fault scenario of Fig.1, when the fault is of SLG type.

Assume the fault of Fig. 1 is asymmetrical and of single line-to-ground (SLG) type. The sequence network corresponding to this fault scenario is shown in Fig. 5, where the subscripts 0, 1, and 2 identify the zero-, positive-, and negative-sequence quantities and parameters [20], [26], [27]. In Fig. 5, the areas *A* and *B* are represented by the corresponding Thevenin equivalent circuits in the sequence domain. Assume the relays at the two ends of the faulted line, i.e., R_A and R_B, utilize NSDEs with the reference directions shown in Fig. 2. The negative-sequence voltage phasors measured by the R_A and the R_B are defined by (7) and (8), respectively [20], [22], [27].

$$V_{R_A} = V_{2A} = -Z_{2A} \times I_{2A} \tag{7}$$

$$V_{R_B} = V_{2B} = -Z_{2B} \times I_{2B} \tag{8}$$

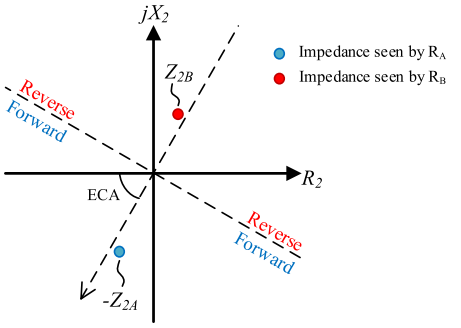

FIGURE 6. Operating characteristics of the NSDE and the negative-sequence impedances seen by R_A and R_B when the fault of Fig. 1 is asymmetrical.

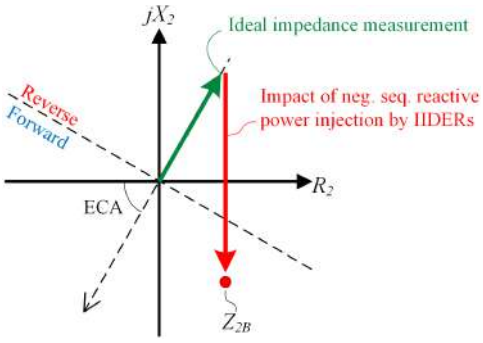

FIGURE 7. Impact of the negative-sequence reactive power injection by IIDERs on the impedance measured by the NSDE during a reverse asymmetrical fault.

The impedances Z_{2A} and Z_{2B} are the Thevenin equivalent negative-sequence impedances of the systems interconnected by the faulted line, hereafter referred to as the system negative-sequence impedances. By analyzing the sequence diagrams associated with line-to-line (LL) and line-to-line-to-ground (LLG) faults, it can be shown that (7) and (8) apply to all asymmetrical faults [6].

The negative-sequence currents measured by R_A and R_B are $I_{R_A} = I_{2A}$ and $I_{R_B} = -I_{2B}$, respectively. Thus, if the fault of Fig. 1 is asymmetrical, the NSDEs of R_A and R_B measure the following impedance angles:

$$\angle V_{R_A} - \angle I_{R_A} = \angle(-Z_{2A}) \tag{9}$$

$$\angle V_{R_B} - \angle I_{R_B} = \pi + \angle(-Z_{2B}) = \angle Z_{2B} \tag{10}$$

The impedances Z_{2A} and Z_{2B} are not fixed and usually not accurately known. However, in traditional transmission systems and distribution networks that are not dominated by inverters, these are typically resistive-inductive impedances with angles close to the line impedance angle $\angle Z_{1L}$. Therefore, the operating characteristic of the NSDE used in traditional power systems is similar to that of the PSDE, except the directional logic of the NSDE is inverted. Whenever the measured negative-sequence impedance is aligned with the $\angle Z_{1L}$, a reverse direction is detected by the NSDE and vice versa [20], [27]. Fig. 6 shows the forward and reverse operating characteristics of the NSDE and the negative-sequence impedances measured by the relays R_A and R_B when the fault of Fig.1 is asymmetrical [22], [23].

The ECA of the NSDE is conventionally set at the line impedance angle $\angle Z_{1L}$, based on a few assumptions that are only valid in traditional power systems. It has been reported that the NSDE may fail to correctly determine the asymmetrical fault direction in the presence of IIDERs [3], [21], [25], [28]. The next part investigates this issue and proposes a simple but effective solution.

C. REVISITING THE NSDE

The practice of setting the ECA of the NSDE at $\angle Z_{1L}$ was initially adopted to maximize the operating torque produced in electromechanical relays. This is the reason that the ECA is also referred to as the maximum torque angle (MTA) [20], [22]. The same strategy is still used in setting modern digital relays, assuming that the angles of the system negative-sequence impedances, i.e., $\angle Z_{2A}$ and $\angle Z_{2B}$, are close to the line impedance angle $\angle Z_{1L}$. This assumption is not necessarily valid in an inverter-dominated microgrid where the measured angles $\angle Z_{2A}$ and $\angle Z_{2B}$ depend on the control strategies of the IIDERs. This issue is theoretically explained below and also demonstrated using simulation results in Section IV.

Under asymmetrical faults, the IIDERs exchange different amounts of negative-sequence reactive current with their host systems, depending on their control and current limiting strategies [8], [9], [25], [29]–[33]. It is shown in [29] that the IIDERs operating based on the voltage support control strategy, e.g., battery energy storage systems (BESS) in the islanded microgrid, can inject considerable amounts of negative-sequence reactive current into the faulted host system. Besides, the studies reported in [9] indicate that the IIDERs operating based on the power control strategy, e.g., photovoltaic (PV) generation system and wind turbines (WT), including those that aim to suppress the negative-sequence current, inject small amounts of negative-sequence reactive current to the faulted host system, due to their harmonic filter capacitors. The reactive behavior of the IIDERs in the negative-sequence domain can change the impedance angles seen by the NSDEs and lead to their malfunction.

Fig. 7 shows the potential impact of the negative-sequence reactive current injected by the IIDERs in the Area *B* on the impedance measured by the NSDE of the R_B, when the fault of Fig. 1 is asymmetrical. As shown in Fig. 7, depending on the sizes, types, and locations of the IIDERs, the resulting shift in the measured negative-sequence impedance can even cause the NSDE to see a reverse fault as a forward fault, if the ECA is set at $\angle Z_{1L}$. The relay R_A could experience similar issues during asymmetrical faults in the islanded microgrid where the strong grid no longer exists and the negative-sequence behavior of the IIDERs in the Area *A* become more impactful.

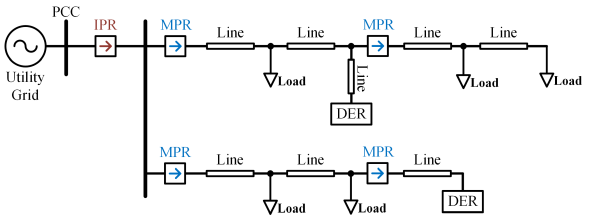

FIGURE 8. Locations and reference directions of the IPR and the MPRs.

Malfunction of the NSDEs due to the impacts of the IIDERs has been reported in [25] and [28], which confirms the above analysis. Application of the ZSDE instead of the NSDE is recommended in [25]. Due to the well-known adverse effects of the zero-sequence mutual coupling on the ZSDE, this is not an ideal solution. Using a smaller non-zero ECA is recommended in [28] to avoid the aforementioned issues. To maximize the reliabilities of the PSDE and the NSDE in the inverter-dominated microgrid, this paper proposes setting the associated ECAs at zero degrees. This results in complete desensitization of these sequence-domain directional elements to the reactive components of the positive- and negative-sequence currents. This strategy enables the PSDE and the NSDE to operate only based on the active power imbalance. The necessity and effectiveness of the proposed solution is verified in Section IV, using comprehensive fault studies performed on a realistic microgrid study system.

III. PROPOSED PROTECTION STRATEGY

The non-pilot protection strategies of [6], [7], [18] utilize an interface protection relay (IPR) at the PCC and multiple microgrid protection relays (MPR) along the microgrid feeder(s). In this section, improved IPR and MPR algorithms are proposed for protection of the inverter-dominated microgrid. Fig. 8 shows the reference directions assumed in this paper for the IPR and the MPRs as well as the locations of the circuit breakers associated with these relays in a typical microgrid. It should be noted that the proposed IPR and MPR are able to operate under faults in either directions, i.e., incorporate independently operating forward and reverse protection functions. The reference directions shown in Fig. 8 are only used to coordinate the relays. The proposed relays utilize a combination of phase- and sequence-domain elements to reliably detect the occurrence of symmetrical and asymmetrical faults. Besides, the fault direction is determined using the improved sequence-domain directional elements, i.e., the PSDE and NSDE with the zero ECA setting, as described in Section II.

The fault current magnitude in an islanded inverter-dominated microgrid does not considerably depend on the fault location. The reason is that the fault current is mainly dictated by the current limits of the inverters [9] and not the fault loop impedance. Hence, the traditional time-current (inverse-time OC) grading strategy does not guarantee coordinated operation of non-pilot protective devices in the inverter-dominated microgrid. The proposed protection strategy is based on the definite-time grading technique of [6], [7], [18], with extra provisions that enable reliable and selective protection of the inverter-dominated microgrid.

A. INTERFACE PROTECTION RELAY

The IPR shown in Fig. 8 must discriminate between internal (forward) and external (reverse) faults and trip the PCC circuit breaker in a timely manner, whenever a fault is detected in either direction. The fault detection criteria and the tripping delay of the IPR depend on the fault type and direction, as described below.

1) PROTECTION AGAINST SYMMETRICAL FAULTS

Under internal symmetrical faults, the fault current contribution from the utility grid is expected to be relatively large for all three phases [7]. Hence, the forward-direction fault timer of the IPR starts once a symmetrical fault is detected by three instantaneous phase OC elements, and a forward fault direction is detected by the improved PSDE. The pickup setting of the OC elements, I_{P-PU}, is set at a value that is higher than (i) two times of the maximum balanced load current, and (ii) the maximum expected motor starting current, seen by the IPR. The IPR trips whenever the timer reaches the threshold TD_{fwd}, i.e., the forward-direction time delay setting.

The response of the inverter-dominated microgrid to external symmetrical faults is drastically different. Due to the limited fault current contributions of the IIDERs, the IPR has to detect external symmetrical faults using Under-Voltage (UV) elements. Hence, the reverse fault timer of the IPR starts once a symmetrical fault is detected by three instantaneous phase UV elements, and a reverse fault direction is detected by the improved PSDE. The pickup setting of the UV element, V_{P-PU}, is set at 50 percent of the rated voltage. The IPR trips whenever the timer reaches the threshold TD_{rev}, i.e., the reverse-direction time delay setting.

2) PROTECTION AGAINST ASYMMETRICAL FAULTS

The IPR detects asymmetrical faults using a negative-sequence OC element [6], [17], [34] which does not react to balanced load currents and thus can use a small pickup setting [34], [35]. A negative-sequence over-voltage (OV) element is also used to enable the IPR to detect resistive asymmetrical faults. The IPR determines the asymmetrical fault direction using the improved NSDE. The forward (reverse) fault timer of the IPR starts once (i) an asymmetrical fault is detected, and (ii) a forward (reverse) fault is indicated by the NSDE.

The pickup setting of the OC element, I_{2-PU}, is set at twice the maximum negative-sequence current caused by unbalanced loads under normal condition. The pickup setting of the OV elements, V_{2-PU}, is set at a value higher than twice the maximum expected negative-sequence voltage

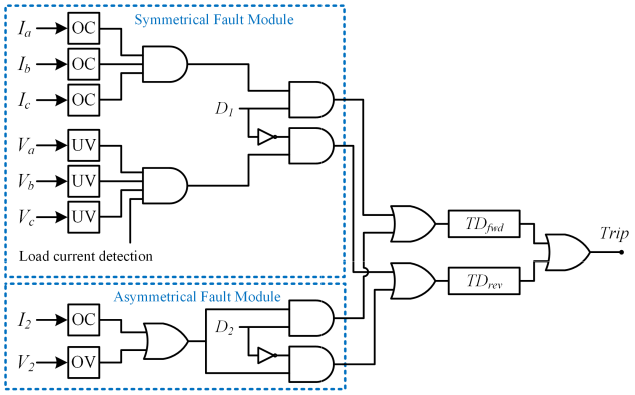

FIGURE 9. Logic diagram of the proposed IPR.

caused by unbalanced loads under normal condition. The IPR trips whenever the forward (reverse) fault timer reaches the threshold TD_{fwd} (TD_{rev}). Fig. 9 shows the logic diagram of the IPR, where D_1 and D_2 represent the output signals of the improved PSDE and NSDE and become *high* under forward symmetrical and asymmetrical faults, respectively.

The "load current detection" signal in Fig. 9 indicates whether the system is energized. This signal is used in the relay logic diagram to prevent the UV elements from unnecessarily tripping the circuit breakers when the system is de-energized.

B. MICROGRID PROTECTION RELAYS

Each MPR is expected to detect the occurrences and directions of internal and external faults and operate in coordination with other protective devices. Due to the reasons explained in the next part, the proposed protection strategy (the IPR) islands the microgrid under any fault, before the first MPR trips. Thus, the MPRs make protective decisions only in the islanded operating conditions, which simplifies the MPR algorithm.

Symmetrical faults in the islanded inverter-dominated microgrid cause the phase voltage magnitudes to drop significantly. Therefore, in the proposed protection strategy, each MPR detects symmetrical faults using instantaneous phase UV elements. The forward (reverse) fault timer of each MPR starts once (i) a symmetrical fault is detected, and (ii) a forward (reverse) fault direction is indicated by the improved PSDE. The MPR trips whenever the forward (reverse) fault timer reaches the threshold TD_{fwd} (TD_{rev}). The pickup setting of the phase UV elements, V_{P-PU}, is set at 50 percent of the rated voltage. For branch lines without DERs, phase OC elements are added to the fault detection logic to prevent false tripping under faults on adjacent feeders/lines [18]. The asymmetrical fault detection algorithm of the MPR is identical to that of the IPR. Fig. 10 shows the logic diagram of the proposed MPR. Similar to the IPR logic diagram of Fig. 9, the MPR logic diagram consists of separate asymmetrical and symmetrical fault detection modules. The MPR trips whenever either of these modules detects a fault and the corresponding timer exceeds a pre-determined delay.

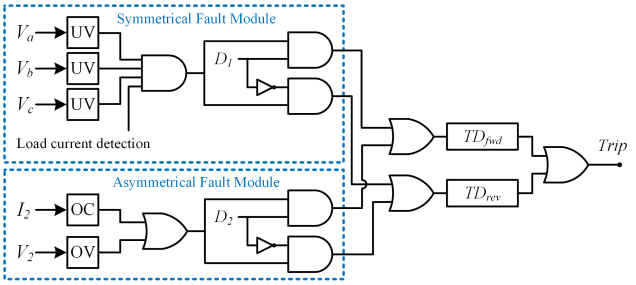

FIGURE 10. Logic diagram of the proposed MPR.

C. PROTECTION COORDINATION

Selective protection of the inverter-dominated microgrid is achieved through coordinated operation of the IPR, the MPRs, and the lateral fuses. Under external faults, the IPR is expected to trip fast, without delaying its operation for coordination with other protective devices. This strategy prevents exposure of the microgrid components to prolonged voltage sags caused by utility grid faults, and also minimizes the risk of islanding a portion of the utility grid (energizing external faults) for an extended period of time. However, to prevent unwanted tripping of the IPR due to system transients, induced voltages, etc., the short delay of $TD_{rev} = 50$ ms is used (Fig. 9).

Under internal faults, the IPR must trip the PCC circuit breaker adequately fast, in order to minimize exposure of the microgrid components to large fault currents. However, instantaneous tripping of the IPR may increase the operation times of the fuses within the microgrid under downstream faults, due to the subsequent drop in the fault current magnitude. When an internal fault takes place, the upstream fuse (if any) is the first protective element to react to the fault. Thereafter, the IPR causes forced islanding. To provide the fuses with sufficient fault clearing time, the IPR utilizes a fixed forward fault delay TD_{fwd} for both symmetrical and asymmetrical faults. The delay is larger than the maximum total clearing time (TCT) of all fuses within the microgrid, in the grid-connected mode. It is determined by applying SLG faults to all fuse-protected laterals, with a reasonably large fault resistance which is assumed to be 40 Ω [36].

After islanding, the MPRs operate in coordination with each other to selectively isolate the faulted feeder/line section, if the internal fault is not cleared by any fuse. The coordinating time interval (CTI) that is utilized to maintain sufficient margin between the operating times of distribution system relays is typically in the range of 0.2 to 0.5 s [1], [26]. In this paper, all relays are coordinated with each other by a CTI of 0.2 s.

IV. STUDY RESULTS

This section presents the results of time-domain simulation studies performed on an inverter-dominated microgrid study

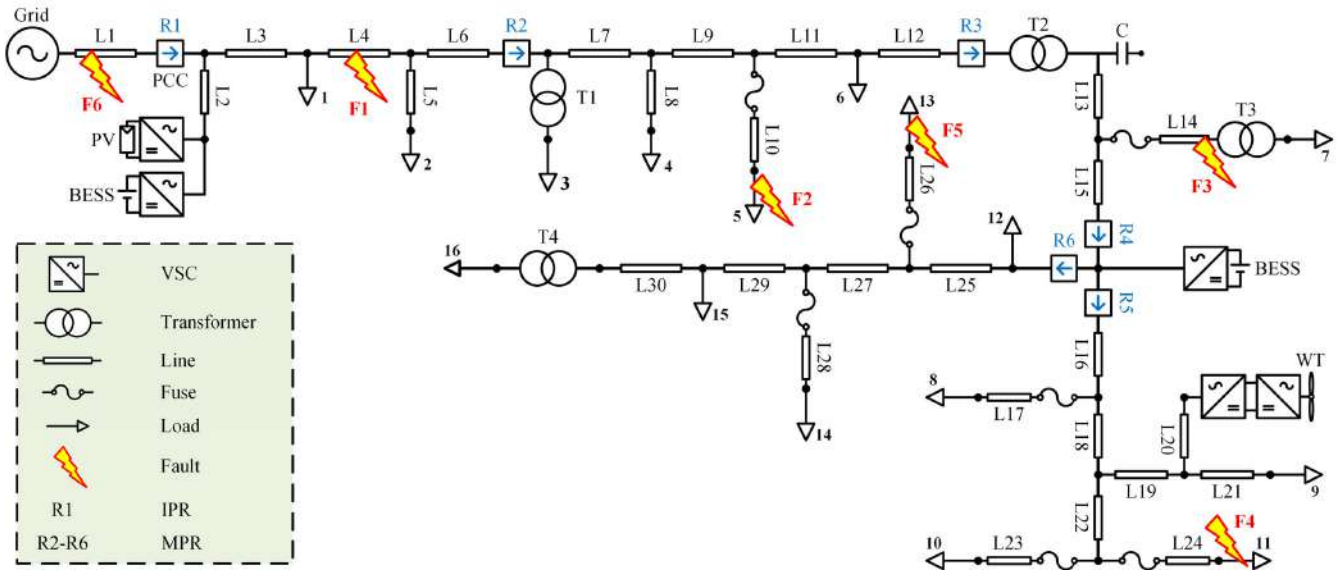

FIGURE 11. Single-line diagram of the inverter-dominated AC microgrid study system.

system in the PSCAD/EMTDC software environment. The study system of Fig. 11 is developed by modifying the Canadian benchmark rural distribution system of [37] to enable its operation as a microgrid. The microgrid includes a PV generation system, a WT, two BESSs, and highly unbalanced loads that are distributed along a 24 km main feeder. All DERs are inverter-interfaced. The DERs and the associated controllers are represented by detailed models, as reported in [38]. The microgrid is assumed to be low-reactance grounded and of the four-wire multi-grounded configuration [19]. The parameters and specifications of the study system components are given in the Appendix. The relay R1 in Fig. 11 is the IPR, and the relays R2-R6 are the MPRs.

The study system is used to demonstrate the adverse effects of IIDERs on the operation of the conventional NSDE and also to verify acceptable performance of the proposed protection strategy that incorporates effective fault detection, fault direction determination, and protection coordination methods. Different types of symmetrical and asymmetrical faults, including LG, LL, LLG, and three-phase faults have been applied to six different locations in the microgrid, shown as F1-F6 in Fig. 11. The fault resistance R_f is assumed to be zero, 10 Ω, and 50 Ω. The microgrid is in the grid-connected steady-state before the faults are applied. The reported relay settings and simulation results are either in per-unit or the primary values, i.e., correspond to the values at the primary-sides of the instrument transformers.

A. NSDE IN THE INVERTER-DOMINATED MICROGRID

The malfunction of the conventional NSDE is demonstrated in this sub-section. Fig. 12 shows the negative-sequence impedances measured by the relays R1-R6, under 99 asymmetrical fault instances with the aforementioned fault types and fault resistances, at the locations F1-F6 shown in Fig. 11, under both grid-connected and islanded modes. To simplify the analysis, the measured impedances are divided into four categories in Fig. 12, depending on the grid-connection mode and the fault location with respect to the relay reference directions. The faults corresponding to the impedances in the shaded areas are seen by the conventional NSDEs as forward faults. Figs. 12(c) and (d) show that the conventional NSDE fails to detect the correct fault direction under a large portion of reverse faults, which confirms the theoretical analysis presented in Section II-C and illustrated in Fig. 7. Fig. 13 shows that the proposed solution, i.e., setting the ECA of the NSDE at zero degrees, effectively resolves the issue. Fig. 13 also demonstrates the necessity of using an ECA setting of zero degrees (or the closest available setting to zero), since any ECA below -15 degrees would cause issues under forward faults, Fig. 13(a), and any ECA above 10 degrees would cause issues under reverse faults, Fig. 13(c).

B. PERFORMANCE OF THE PROPOSED PROTECTION STRATEGY

This part evaluates the performance of the proposed non-pilot protection strategy applied to the study system of Fig. 11. The relays R1-R6 are coordinated with each other and with the downstream fuses, according to the strategy introduced in part III-C. Coordination of the forward and reverse elements of the relays is performed separately, as follows:

Forward-directional elements: R2→R3→(R5& R6)→R1
Reverse-directional elements: R5→R4→R3→R2→R1

The notation Rj →Rk means that, for any fault that is seen by the Rj and the Rk in the same direction, the relay Rj operates with a larger delay as compared with the Rk. It should be noted that the R1 operates faster than all relays in both directions, because it is designated as the IPR and

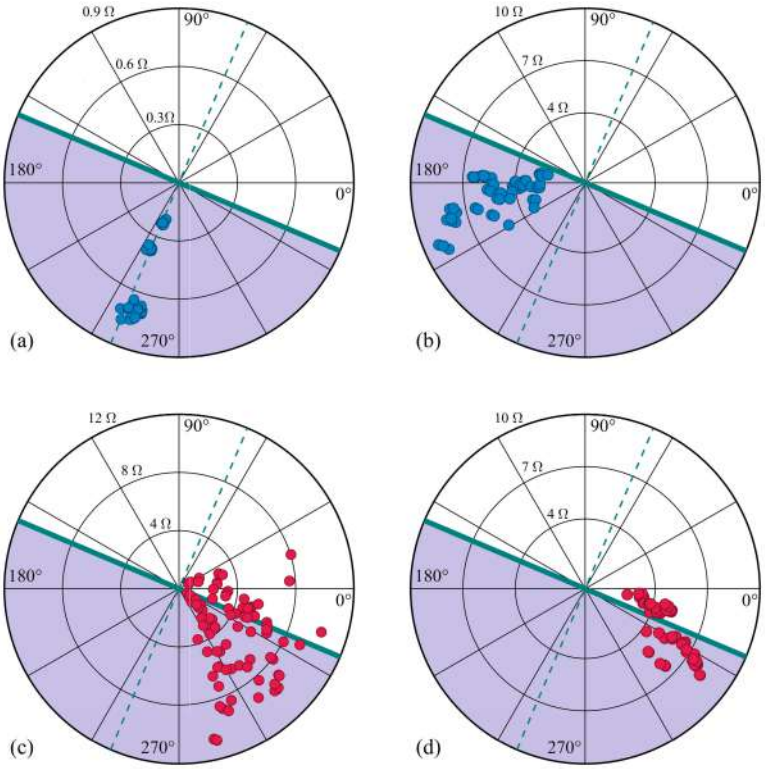

FIGURE 12. Operating characteristics of the conventional NSDE, and the negative-sequence impedances measured by relays R1-R6, under (a) forward faults in the grid-connected microgrid, (b) forward faults in the islanded microgrid, (c) reverse faults in the grid-connected microgrid, and (d) reverse faults in the islanded microgrid.

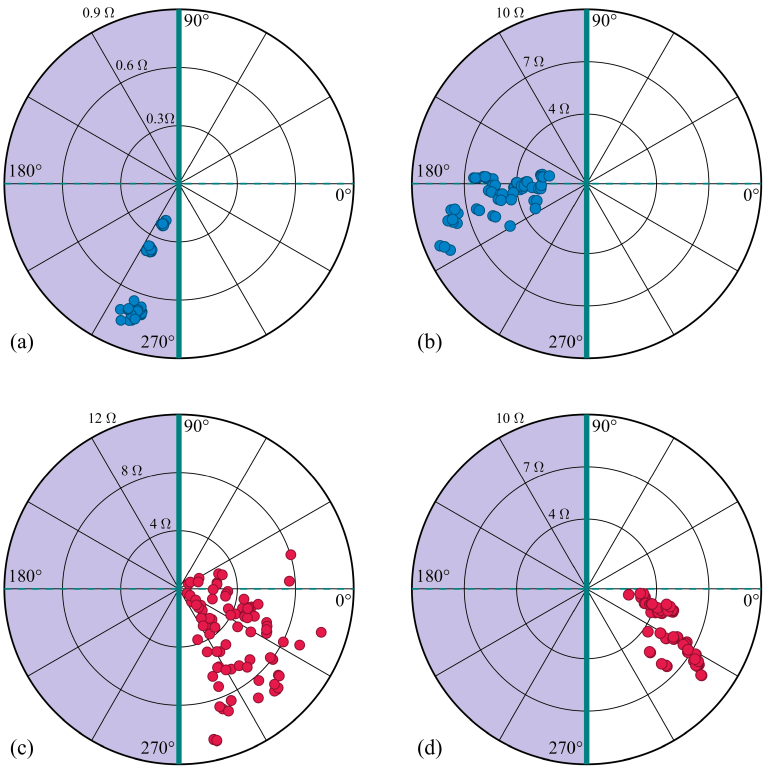

FIGURE 13. Operating characteristics of the proposed NSDE, and the negative-sequence impedances measured by relays R1-R6, under (a) forward faults in the grid-connected microgrid, (b) forward faults in the islanded microgrid, (c) reverse faults in the grid-connected microgrid, and (d) reverse faults in the islanded microgrid.

TABLE 1. Relay types and settings.

Relay	Type	TD_{fwd} (ms)	TD_{rev} (ms)	Pick Up Settings			
				$I_{P\text{-}PU}$ (A)	$V_{P\text{-}PU}$ (p.u.)	$I_{2\text{-}PU}$ (A)	$V_{2\text{-}PU}$ (p.u.)
R1	IPR	200	50	800	0.5	32	0.1
R2	MPR	800	250	-	0.5	28	0.1
R3	MPR	600	450	-	0.5	16	0.1
R4	MPR	-	650	-	0.5	16	0.1
R5	MPR	400	850	-	0.5	8	0.1
R6	MPR	400	-	-	0.5	8	0.1

must always trip before all MPRs. The relay R6 does not include a reverse directional elements, because it is installed on a passive branch that would never feed reverse faults. The relay R4 does not include a forward directional element due to the presence of the R6 and the R5 on the same bus. A forward element in the R4 would be redundant and would increase the forward operating times of the R3 and the R2 by 200 ms. The relays R1-R6 are coordinated with each other and with the lateral fuses, according to the coordination strategy described in Section III-C. The relay settings are shown in Table 1.

Faults of different types with various resistances are applied to different locations under both grid-connected and islanded operating modes of the microgrid. Table 2 shows the operating time delays of the relays and the TCTs of the fuses that protect the faulted laterals (if applicable), for internal faults. Table 3 shows the relay operating time delays under external faults.

The study results indicate that the proposed protection strategy selectively and reliably protects the microgrid under the grid-connected and islanded modes and various fault conditions. For the cases where the fault is applied to a lateral circuit protected by a fuse, i.e. the faults F2-F5 in Fig. 11, the corresponding lateral fuse is the first protective device that operates, as shown in Table 2.

Table 2 also shows that the reduced fault current level in the islanded microgrid increases the fuse TCTs. However, in both grid-connected and islanded modes, the minimum margin of about 200 ms is maintained between the operation times of all protective devices that see the fault in the same direction. The reason is that the relays are coordinated with the fuses, taking into account the fault current variations in both operation modes of the microgrid.

The proposed protection strategy enables fuse protection of the lateral circuits, provided that the current ratings of the fuses are below the fault current magnitude in the islanded inverter-dominated microgrid. However, if fuses with significantly higher current ratings are utilized (in case the loads protected by the fuses are considerably larger), the limited fault current magnitude in the islanded inverter-dominated microgrid may not be sufficiently large to enable fuse operation in a timely manner. Under such conditions, the fuses merely operate in the grid-connected mode, and the islanded microgrid is protected by the relays. It should be noted that this is not a shortcoming of the proposed protection strategy, because changing the relay operating times would not enable the fuses to operate in such conditions. To maximize the sensitivity of each fuse to faults in the islanded inverter-dominated microgrid, application of fuses with unnecessarily large current ratings should be avoided.

The maximum operating time of all protective devices under the investigated fault conditions is about 1205 ms. The aforementioned delay is due to the fact that six relays are coordinated with each other and with the lateral fuses in the study system of Fig. 11. These numerous protective devices are intentionally utilized in this study system to demonstrate the capabilities of the proposed protection strategy. However, fewer relays are typically utilized on a microgrid feeder, which reduces the maximum relay operation time. In addition, even in the study system of Fig. 11, none of the faults F1-F5 would remain uncleared for such long time periods unless multiple protective devices fail to operate.

It should be noted that the proposed protection strategy is not designed to achieve the highest speed among the existing microgrid protection strategies. The existing communication-based protection strategies typically operate faster. The main contribution of this paper is that the proposed protection strategy enables reliable and selective protection of the inverter-dominated microgrid, with reasonable speed, without utilizing communication systems. The proposed protection strategy is suitable for inverter-dominated microgrids where application of communication systems is not feasible due to practical or economic reasons. In addition, the proposed protection strategy can be utilized as backup for the communication-assisted protection schemes.

The IPR and MPR algorithms of Figs. 9 and 10 are implemented in an off-the-shelf commercial relay [39] and evaluated using an industrial relay testing platform [40]. The voltage and current signals obtained by simulating various fault scenarios are loaded to the relay testing device which sends the recorded signals to the relay, as shown in Fig. 14. The MPR and IPR algorithms are implemented in the relay by appropriately setting the parameters of the available phase- and sequence-domain protective elements as well as defining new Logic Variables (LVs) and variable timers. The graphical logic diagram of Fig. 15 is created by the user interface software of the relay manufacturer and shows how the aforementioned LVs and timers are integrated with the internal protective elements of the relay to create the MPR algorithm.

The performance of the relay is evaluated under various fault scenarios by reading the event files recorded by the relay after the test signals are played back to the relay by the testing device. The investigation verifies that the proposed microgrid protection strategy can be implemented in an off-the-shelf digital relay, and the performance of the relay matches with the results obtained by PSCAD simulation.

TABLE 2. Relay and fuse operating time delays for internal faults.

Fault			Operation time (ms)												
			Grid-connected mode							Islanded mode					
Location	Type	R_f	R1	R2	R3	R4	R5	R6	Fuse	R2	R3	R4	R5	R6	Fuse
F1	AG	0	205	256	455	656	856	N/A	N/A	253	452	653	852	N/A	N/A
		10	206	263	459	663	893	N/A	N/A	258	453	654	853	N/A	N/A
		50	207	555	755	955	1169	N/A	N/A	260	458	659	859	N/A	N/A
	AB	0	203	253	453	653	853	N/A	N/A	256	452	655	856	N/A	N/A
		10	203	254	453	655	855	N/A	N/A	256	456	656	856	N/A	N/A
		50	204	554	755	955	1171	N/A	N/A	257	456	657	857	N/A	N/A
	ABG	0	202	253	453	654	853	N/A	N/A	257	457	657	857	N/A	N/A
		10	202	264	486	688	884	N/A	N/A	258	457	658	858	N/A	N/A
		50	212	596	785	985	1205	N/A	N/A	266	465	665	866	N/A	N/A
	ABC	0	234	269	459	662	862	N/A	N/A	259	459	659	859	N/A	N/A
F2	AG	0	206	805	455	656	873	N/A	22	803	452	653	852	N/A	76
		10	206	806	456	657	890	N/A	35	808	452	654	853	N/A	97
		50	208	826	500	718	1170	N/A	153	812	458	659	859	N/A	256
	AB	0	203	803	453	653	853	N/A	16	807	452	655	856	N/A	210
		10	203	803	453	654	853	N/A	23	807	455	656	856	N/A	239
		50	204	832	497	698	899	N/A	75	809	456	657	857	N/A	252
	ABG	0	202	822	453	654	853	N/A	15	815	457	657	857	N/A	102
		10	203	822	460	662	860	N/A	27	815	457	658	858	N/A	139
		50	212	940	782	985	1205	N/A	142	822	465	665	865	N/A	268
	ABC	0	207	815	469	659	859	N/A	14	809	459	659	859	N/A	207
F3	AG	0	206	806	606	655	872	N/A	33	803	603	653	852	N/A	81
		10	206	806	606	656	875	N/A	47	808	604	654	853	N/A	101
		50	208	847	628	683	896	N/A	172	812	610	658	859	N/A	263
	AB	0	204	804	603	653	853	N/A	26	807	606	655	856	N/A	212
		10	204	804	603	654	853	N/A	33	808	606	656	856	N/A	244
		50	205	805	604	660	876	N/A	88	809	607	657	857	N/A	257
	ABG	0	203	803	602	654	854	N/A	24	815	607	657	857	N/A	106
		10	204	838	602	655	856	N/A	36	815	607	658	857	N/A	142
		50	213	922	634	988	1198	N/A	151	822	615	665	865	N/A	262
	ABC	0	212	1106	897	663	863	N/A	22	809	609	659	859	N/A	195
F4	AG	0	207	806	606	N/A	402	N/A	45	804	604	N/A	403	N/A	91
		10	207	824	606	N/A	405	N/A	61	808	608	N/A	403	N/A	114
		50	208	847	628	N/A	423	N/A	194	812	610	N/A	404	N/A	284
	AB	0	204	804	603	N/A	403	N/A	36	808	606	N/A	406	N/A	213
		10	204	804	603	N/A	403	N/A	44	808	606	N/A	406	N/A	247
		50	205	805	604	N/A	403	N/A	103	810	607	N/A	406	N/A	267
	ABG	0	204	804	603	N/A	402	N/A	32	815	607	N/A	406	N/A	118
		10	204	821	603	N/A	402	N/A	44	816	608	N/A	407	N/A	154
		50	213	918	634	N/A	434	N/A	167	822	615	N/A	408	N/A	277
	ABC	0	216	1113	907	N/A	415	N/A	29	813	613	N/A	412	N/A	216
F5	AG	0	206	806	606	N/A	872	405	32	803	603	N/A	852	402	81
		10	206	806	606	N/A	875	405	47	808	604	N/A	853	402	102
		50	208	846	628	N/A	896	424	181	812	610	N/A	859	402	276
	AB	0	204	804	603	N/A	853	402	26	807	606	N/A	856	402	209
		10	204	804	603	N/A	853	402	34	808	606	N/A	856	405	242
		50	205	805	604	N/A	876	402	90	809	607	N/A	857	406	261
	ABG	0	203	823	620	N/A	854	420	24	815	607	N/A	857	402	105
		10	204	838	602	N/A	856	401	36	815	607	N/A	857	402	143
		50	213	922	634	N/A	1198	433	158	822	615	N/A	865	406	274
	ABC	0	212	1107	897	N/A	863	413	22	809	609	N/A	859	409	195

TABLE 3. Relay operating time delays for external faults.

Fault			Operation time (ms)				
Location	Type	R_f	R1	R2	R3	R4	R5
F6	AG	0	56	257	456	657	888
		10	64	267	463	666	896
		50	154	364	564	763	977
	AB	0	53	253	453	653	853
		10	54	256	456	660	875
		50	152	354	554	754	966
	ABG	0	53	253	453	653	853
		10	60	364	522	739	936
		50	176	397	577	797	994
	ABC	0	59	259	459	662	862

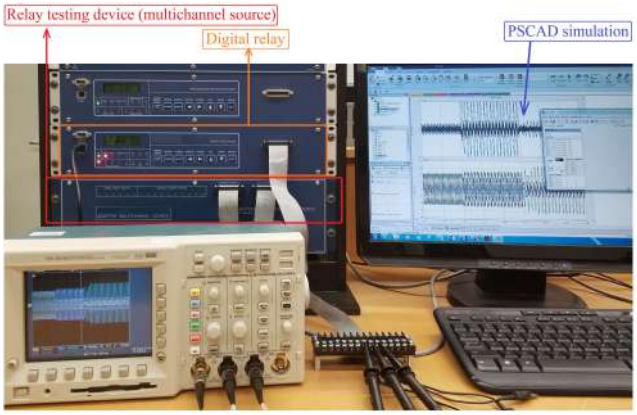

FIGURE 14. Hardware setup for implementing the proposed protection strategy in an off-the-shelf digital relay and testing its performance under the fault scenarios of Tables 2 and 3.

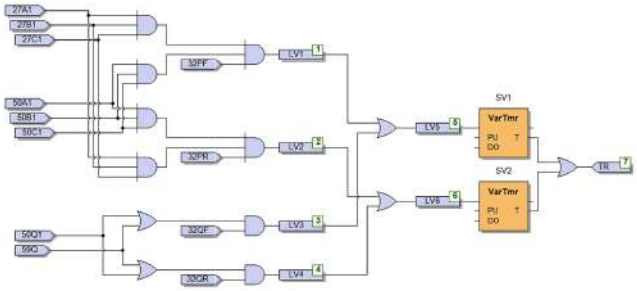

FIGURE 15. Graphical logic representation of the MPR algorithm implemented in the digital relay shown in Fig. 14, which is shown by the user interface software provided by the relay manufacturer.

V. CONCLUSION

This paper introduces a non-pilot protection strategy for the inverter-dominated microgrid. The study results indicate that the proposed protection strategy:

- enables reliable detection of symmetrical and asymmetrical faults, reliable identification of the fault direction, and selective protection under both grid-connected and islanded operation modes.
- enables fuse protection of lateral circuits.
- prevents microgrid exposure to prolonged fault currents from the utility grid, under internal faults.
- minimizes microgrid exposure to voltage sags during utility grid faults.

TABLE 4. Study system parameters.

Component	Description
Grid	$V_{LL\text{-}base}$ = 27.6 kV, SSC = 885.33 MVA, X/R = 10
Wind Turbine	S_{WT} = 4 MVA = 2×2 MVA
PV power plant	S_{PV} = 3.5 MVA
BESS units	S_{BESS} = 2×2 MVA
Capacitor bank	Q = 1.5 MVAR
Transformers	T1: 3.6 MVA, X = 6 p.u., 27.6 kV/8.31 kV, ΔY T2: 15 MVA, X = 7.3 p.u., 27.6 kV/27.6 kV, YY T3: 1 MVA, X = 4 p.u., 27.6 kV/8.31 kV, ΔY T4: 3.6 MVA, X = 5.65 p.u., 27.6 kV/8.31 kV, ΔY
Overhead lines	Spacing ID = STD-3PH-NBP [41] R_1 = 0.172 Ω/km, R_0 = 0.491 Ω/km X_1 = 0.404 Ω/km, X_0 = 1.354 Ω/km B_1 = 4.171 uS/km, B_0 = 1.759 uS/km
Fuses	20A-E, BA2 Type Expulsion Fuse [42]

TABLE 5. Line parameters.

Line	Length (m)	Line	Length (m)	Line	Length (m)
L1	5700	L11	3330	L21	1550
L2	1010	L12	1030	L22	2120
L3	400	L13	3490	L23	1820
L4	380	L14	1430	L24	2540
L5	120	L15	190	L25	620
L6	170	L16	1940	L26	3580
L7	260	L17	2450	L27	770
L8	140	L18	1630	L28	2080
L9	940	L19	1200	L29	4510
L10	300	L20	820	L30	4040

TABLE 6. Load specifications.

Load Name	Phase A (kVA)	Phase B (kVA)	Phase C (kVA)	Power Factor
1	731.22	741.22	891.22	0.95
2	115.33	115.33	115.33	0.87
3	1099.00	946.00	1310.00	0.95
4	85.33	85.33	85.33	0.75
5	2.10	2.10	2.10	1
6	186.67	41.67	36.67	0.95
7	216.67	216.67	216.67	1
8	0.00	50.00	0.00	0.95
9	160.00	0.00	0.00	0.95
10	0.00	0.00	205.00	1
11	146.67	126.67	171.67	0.95
12	10.00	0.00	0.00	0.95
13	0.00	0.00	215.00	0.95
14	0.00	85.00	0.00	0.95
15	60.00	0.00	50.00	0.95
16	749.00	710.00	821.00	0.95

- can be implemented using the existing commercial relays.

Although the proposed protection strategy is devised to achieve improved performance in inverter-dominated microgrids, it is also applicable to microgrids that contain rotating machines instead of inverters. However, in systems that do not suffer from the issues associated with the inverter-dominated microgrids, higher protection speed can

be achieved by using the traditional protection coordination method.

APPENDIX

See Tables 3–6.

REFERENCES

[1] H. M. Sharaf, H. H. Zeineldin, and E. El-Saadany, "Protection coordination for microgrids with grid-connected and islanded capabilities using communication assisted dual setting directional overcurrent relays," *IEEE Trans. Smart Grid*, vol. 9, no. 1, pp. 143–151, Jan. 2018.

[2] Z. Chen, X. Pei, M. Yang, L. Peng, and P. Shi, "A novel protection scheme for inverter-interfaced microgrid (IIM) operated in islanded mode," *IEEE Trans. Power Electron.*, vol. 33, no. 9, pp. 7684–7697, Sep. 2018.

[3] A. Hooshyar and R. Iravani, "Microgrid protection," *Proc. IEEE*, vol. 105, no. 7, pp. 1332–1353, Jul. 2017.

[4] A. A. Memon and K. Kauhaniemi, "A critical review of AC microgrid protection issues and available solutions," *Electr. Power Syst. Res.*, vol. 129, pp. 23–31, Dec. 2015.

[5] S. Mirsaeidi, D. M. Said, M. W. Mustafa, M. H. Habibuddin, and K. Ghaffari, "An analytical literature review of the available techniques for the protection of micro-grids," *Int. J. Elect. Power Energy Syst.*, vol. 58, pp. 300–306, Jun. 2014.

[6] S. F. Zarei and M. Parniani, "A comprehensive digital protection scheme for low-voltage microgrids with inverter-based and conventional distributed generations," *IEEE Trans. Power Del.*, vol. 32, no. 1, pp. 441–452, Feb. 2017.

[7] M. A. Zamani, A. Yazdani, and T. S. Sidhu, "A communication-assisted protection strategy for inverter-based medium-voltage microgrids," *IEEE Trans. Smart Grid*, vol. 3, no. 4, pp. 2088–2099, Dec. 2012.

[8] W.-M. Guo, L.-H. Mu, and X. Zhang, "Fault models of inverter-interfaced distributed generators within a low-voltage microgrid," *IEEE Trans. Power Del.*, vol. 32, no. 1, pp. 453–461, Feb. 2017.

[9] Z. Shuai, C. Shen, X. Yin, X. Liu, and J. Shen, "Fault analysis of inverter-interfaced distributed generators with different control schemes," *IEEE Trans. Power Del.*, vol. 33, no. 3, pp. 1223–1235, Jun. 2018.

[10] E. Sortomme, S. S. Venkata, and J. Mitra, "Microgrid protection using communication-assisted digital relays," *IEEE Trans. Power Del.*, vol. 25, no. 4, pp. 2789–2796, Oct. 2010.

[11] H. Muda and P. Jena, "Superimposed adaptive sequence current based microgrid protection: A new technique," *IEEE Trans. Power Del.*, vol. 32, no. 2, pp. 757–767, Apr. 2017.

[12] H. Laaksonen, D. Ishchenko, and A. Oudalov, "Adaptive protection and microgrid control design for Hailuoto island," *IEEE Trans. Smart Grid*, vol. 5, no. 3, pp. 1486–1493, May 2014.

[13] P. Mahat, Z. Chen, B. Bak-Jensen, and C. L. Bak, "A simple adaptive overcurrent protection of distribution systems with distributed generation," *IEEE Trans. Smart Grid*, vol. 2, no. 3, pp. 428–437, Sep. 2011.

[14] H. F. Habib, C. R. Lashway, and O. A. Mohammed, "A review of communication failure impacts on adaptive microgrid protection schemes and the use of energy storage as a contingency," *IEEE Trans. Ind. Appl.*, vol. 54, no. 2, pp. 1194–1207, Mar./Apr. 2018.

[15] H. Al-Nasseri, M. A. Redfern, and F. Li, "A voltage based protection for micro-grids containing power electronic converters," in *Proc. IEEE PES Gen. Meeting*, Montreal, QC, Canada, Jun. 2006, pp. 1–7.

[16] D. P. Mishra, S. R. Samantaray, and G. Joos, "A combined wavelet and data-mining based intelligent protection scheme for microgrid," *IEEE Trans. Smart Grid*, vol. 7, no. 5, pp. 2295–2304, Sep. 2016.

[17] H. Nikkhajoei and R. H. Lasseter, "Microgrid protection," in *Proc. IEEE PES Gen. Meeting*, Tampa, FL, USA, Jun. 2007, pp. 1–6.

[18] M. A. Zamani, T. S. Sidhu, and A. Yazdani, "A protection strategy and microprocessor-based relay for low-voltage microgrids," *IEEE Trans. Power Del.*, vol. 26, no. 3, pp. 1873–1883, Jul. 2011.

[19] J. Mohammadi, F. B. Ajaei, and G. Stevens, "Grounding the AC microgrid," *IEEE Trans. Ind. Appl.*, vol. 55, no. 1, pp. 98–105, Jul. 2018.

[20] J. Roberts and A. Guzman, "Directional element design and evaluation," in *Proc. SEL*, Pullman, WA, USA, 2006, pp. 1–27.

[21] A. Hooshyar and R. Iravani, "A new directional element for microgrid protection," *IEEE Trans. Smart Grid*, vol. 9, no. 6, pp. 6862–6876, Jul. 2017.

[22] J. Horak, "Directional overcurrent relaying (67) concepts," in *Proc. 59th Annu. Conf. Protective Relay Eng.*, College Station, TX, USA, Aug. 2006, pp. 1–13.

[23] J. Horak and W. Babic, "Directional overcurrent relaying (67) concepts," in *Proc. IEEE Rural Electr. Power Conf.*, Albuquerque, NM, USA, Apr. 2006, pp. 1–8.

[24] D. Jones and J. J. Kumm, "Future distribution feeder protection using directional overcurrent elements," *IEEE Trans. Ind. Appl.*, vol. 50, no. 2, pp. 1385–1390, Mar./Apr. 2014.

[25] M. Nagpal and C. Henville, "Impact of power-electronic sources on transmission line ground fault protection," *IEEE Trans. Power Del.*, vol. 33, no. 1, pp. 62–70, Feb. 2018.

[26] S. H. Horowitz, and A. G Phadke, *Protective Relaying Theory and Applications*. New York, NY, USA: Marcel Dekker, 2004.

[27] F. Calero, "Rebirth of negative-sequence quantities in protective relaying with microprocessor-based relays," in *Proc. 57th Annu. Conf. Protective Relay Eng.*, College Station, TX, USA, Apr. 2004, pp. 190–219.

[28] B. Chen, A. Shrestha, F. A. Ituzaro, and N. Fischer, "Addressing protection challenges associated with Type 3 and Type 4 wind turbine generators," in *Proc. 68th Annu. Conf. Protective Relay Eng.*, College Station, TX, USA, Mar. 2015, pp. 335–344.

[29] J. Jia, G. Yang, and A. H. Nielsen, "A review on grid-connected converter control for short-circuit power provision under grid unbalanced faults," *IEEE Trans. Power Del.*, vol. 33, no. 2, pp. 649–661, Apr. 2018.

[30] A. Camacho, M. Castilla, J. Miret, A. Borrell, and L. G. de Vicuña, "Active and reactive power strategies with peak current limitation for distributed generation inverters during unbalanced grid faults," *IEEE Trans. Ind. Electron.*, vol. 62, no. 3, pp. 1515–1525, Mar. 2015.

[31] T. Neumann, T. Wijnhoven, G. Deconinck, and I. Erlich, "Enhanced dynamic voltage control of type 4 wind turbines during unbalanced grid faults," *IEEE Trans. Energy Convers.*, vol. 30, no. 4, pp. 1650–1659, Dec. 2015.

[32] T. Wijnhoven, G. Deconinck, T. Neumann, and I. Erlich, "Control aspects of the dynamic negative sequence current injection of type 4 wind turbines," in *Proc. IEEE PES Gen. Meeting*, National Harbor, MD, USA, Jul. 2014, pp. 1–5.

[33] M. S. El Moursi, W. Xiao, and J. L. Kirtley, "Fault ride through capability for grid interfacing large scale PV power plants," *IET Gener., Transmiss. Distrib.*, vol. 7, no. 9, pp. 1027–1036, Sep. 2013.

[34] A. F. Elneweihi, E. O. Schweitzer, III, and M. W. Feltis, "Negative-sequence overcurrent element application and coordination in distribution protection," *IEEE Trans. Power Del.*, vol. 8, no. 3, pp. 915–924, Jul. 1993.

[35] S. Lotfi-fard, J. Faiz, and R. Iravani, "Improved overcurrent protection using symmetrical components," *IEEE Trans. Power Del.*, vol. 22, no. 2, pp. 843–850, Apr. 2007.

[36] "Distribution system feeder overcurrent protection," GE Power Manage. Company, Markham, ON, Canada, Tech. Rep. GET-6450, 1979.

[37] T. K. Abdel-Galil, A. E. B. Abu-Elanien, E. F. El-Saadany, A. Girgis, Y. A. R. I. Mohamed, M. M. A. Salama, and H. H. M. Zeineldin, "Protection coordination planning with distributed generation," NRCAN, Varennes, QC, Canada, Tech. Rep. CETC 2007-149/2007-09-14, Jun. 2007.

[38] H. Lahiji, J. Mohammadi, F. B. Ajaei, and R. Boudreau, "Damping power oscillations in the inverter-dominated microgrid," in *Proc. 18th Ann. IEEE Canada Elect. Power Energy Conf.*, Toronto, ON, Canada, Oct. 2018, pp. 1–7.

[39] *SEL351-5, -6, -7 Protection Systems, Instruction Manual*, Schweitzer Eng. Lab., Pullman, WA, USA, 2019.

[40] *SEL-RTS Relay Test System, Instruction Manual*, Schweitzer Eng. Lab., Pullman, WA, USA, Feb. 1997.

[41] E. Abbasi, "Typical Canadian medium voltage benchmark network model for integration of distributed energy resources," in *Proc. CIGRE*, Vancouver, BC, Canada, Oct. 2016, pp. 1–8.

[42] *Medium Voltage Expulsion Fuses, BA/DBA Fuse Units, Datasheet*, Eaton, Dublin, Ireland, Aug. 2011.

HOUMAN LAHIJI (S'17–M'18) received the B.Sc. degree in electrical engineering from the University of Manitoba, Canada, in 2016, and the M.E.Sc degree in electrical engineering from Western University, Canada, in 2018.

He is currently a Renewable Energy Consultant with Phoventus Inc., ON, Canada. His research interest includes protection and control of power systems with a focus on renewable energy and microgrids.

FIROUZ BADRKHANI AJAEI (S'12–M'15) received the B.Sc. degree from Tehran Polytechnic University, Iran, in 2006, the M.Sc. degree from the University of Tehran, Iran, in 2009, and the Ph.D. degree from the University of Toronto, Canada, in 2015, all in electrical engineering.

He is currently an Assistant Professor with the Department of Electrical and Computer Engineering, Western University, Canada. His research interests include protection and control of power systems with a focus on renewable energy systems, microgrids, and HVdc–ac grids.

RYAN E. BOUDREAU received the bachelor's degree in electrical engineering from the Technical University of Nova Scotia, Halifax, NS, Canada, in 1999. He is currently a Protection and Automation Manager with Hydro One Networks Inc., Toronto, ON, Canada, responsible for distribution P&C, distribution modernization, and DER assessments. His previous work experiences include field operations, distribution asset management, and distributed generation connection and commissioning with Nova Scotia Power Inc. and connection impact assessments with Hydro One Networks Inc.